Journal of Materials Chemistry A

PAPER

Cite this: J. Mater. Chem. A, 2018, 6, 3500

A self-powered flexible hybrid piezoelectric–pyroelectric nanogenerator based on non-woven nanofiber membranes†

Ming-Hao You,[a] Xiao-Xiong Wang,[a] Xu Yan,[ab] Jun Zhang,[a] Wei-Zhi Song,[a] Miao Yu,[ac] Zhi-Yong Fan,[d] Seeram Ramakrishna[e] and Yun-Ze Long*[ab]

Received 19th November 2017
Accepted 16th January 2018

DOI: 10.1039/c7ta10175a

rsc.li/materials-a

Self-powered systems based on nanogenerators (NGs) that are capable of harvesting mechanical and thermal energies for electricity and are obtained using low-cost materials and simple preparation methods have received great attention. Herein, we report a lightweight and flexible self-powered hybrid NG based on the piezoelectric and pyroelectric effects of an electrospun non-woven poly(vinylidene fluoride) (PVDF) nanofiber membrane (NFM), which can be directly used as an active layer without any post-poling treatment. The flexibility of the NG was enhanced by using an electrospun thermoplastic polyurethane (TPU) NFM as a substrate and a conductive PEDOT:PSS-PVP NFM and a carbon nanotube layer as the electrodes. The capabilities of the NFM to harvest mechanical and thermal energies were demonstrated. Mechanical impacting and bending can effectively stimulate the piezoelectric output of the NG, which can directly light a LED. Moreover, a hybrid piezoelectric–pyroelectric current of the NG was detected upon simultaneous application of strain and a thermal gradient. Due to its flexible non-woven structure, the NG can further harvest energy from body motion and cold/hot airflows. Furthermore, its mechanical durability, robustness and practicality were investigated by charging a capacitor. The novel design of the NFM-constructed hybrid NG demonstrated here can be applied not only to self-powered wearable electronic textiles but also to power generation on a large scale.

1. Introduction

The conversion of environmental energy into electrical energy has attracted much attention in recent years because of the rapidly increasing energy demands for personal electronic devices.[1–8] As an effective method to harvest the surrounding local energy in our daily life into electricity, especially for self-powered systems,[9–13] nanogenerators (NGs) have been invented and have shown a wide range of potential applications, such as airflow/wind disturbance power generation[14–18] and flexible electronic skins;[19] they are especially suitable for use in wearable self-powered electronics.[20–27] Taking into account their practicality, it is expected that NGs which are flexible, lightweight, durable, and can individually or simultaneously scavenge mechanical and thermal energies will be explored.

Recently, flexible hybrid NGs based on piezoelectric and pyroelectric effects that can effectively harvest mechanical and thermal energies have received great attention. For example, Ko *et al.* reported a hybrid NG using $Pb(Zr_{0.52}Ti_{0.48})O_3$ film and $LaNiO_3$/Pt electrodes.[14] Lee *et al.* reported a micro-patterned poly(vinylidenefluoride-*co*-trifluoroethylene) film-based hybrid NG with a micro-patterned polydimethylsiloxane–carbon nanotubes (CNTs) composite and graphene nanosheets electrodes.[28] However, the processes of fabricating these NGs are difficult and cumbersome; this presents challenges to their mass production and practical application.

Based on a simple nanofiber preparation technology, namely electrospinning, NGs with flexible non-woven structures have emerged; electrospun poly(vinylidene fluoride) (PVDF) nanofiber membranes (NFMs)[29,30] combined with conductive NFMs may be a good choice to fabricate flexible hybrid NGs. PVDF NFMs produced by electrospinning can be directly used for energy harvesting without any additional treatment. This is because during the electrospinning process, the applied high voltage, rapid evaporation of the solvent, and high stretching ratio of the PVDF solution jet benefit crystallization in the β-phase, which possesses the most favourable piezoelectric and

[a]Collaborative Innovation Center for Nanomaterials & Devices, College of Physics, Qingdao University, Qingdao 266071, China. E-mail: yunze.long@163.com; yunze.long@qdu.edu.cn

[b]Industrial Research Institute of Nonwovens & Technical Textiles, Qingdao University, Qingdao 266071, China

[c]Department of Mechanical Engineering, Columbia University, New York, NY 10027, USA

[d]Department of Electronic & Computer Engineering, The Hong Kong University of Science & Technology, Kowloon, Hong Kong, China

[e]Center for Nanofibers & Nanotechnology, Nanoscience & Nanotechnology Initiative, Faculty of Engineering, National University of Singapore, Singapore

† Electronic supplementary information (ESI) available. See DOI: 10.1039/c7ta10175a

pyroelectric properties.[31,32] In addition, under the induction of an electrospinning electric field, the average preferential electro-active dipoles orientate along the thickness direction of the PVDF NFM.[33] Moreover, continuous and large-scale NFMs can be prepared by electrospinning methods.

In this work, we report the innovative design of a flexible hybrid NG based on an electrospun PVDF NFM, a thermoplastic polyurethane (TPU) NFM–carbon nanotubes (CNTs) composite, and an electrospun poly(3,4-ethylenedioxythiophene):poly(styrene sulfonate)-polyvinyl pyrrolidone (PEDOT:PSS-PVP) conductive NFM (CNFM), which were assembled into a self-powered nonwoven NG. The TPU NFM–CNTs was used as a substrate and the bottom electrode of the NG to improve its flexibility. The PEDOT:PSS-PVP CNFM served as a flexible top electrode. The piezoelectricity electrical output of the NG induced by mechanical compression and bending was tested, and the pyroelectric electrical output of the NG was also successfully measured. Furthermore, hybrid piezoelectric and pyroelectric output was detected, and the applications of harvesting energy from human motions and cold/hot airflows were discussed. These results indicate the potential applications of this hybrid NG in self-powered nonwoven devices.

2. Experimental

2.1 Materials

PVDF powder (M_w: 550 000, Shanghai 3F New material co., Ltd.), thermoplastic polyurethane (TPU, K985A, Jiangsu Kesu Import & Export co., Ltd.), polyvinylpyrrolidone (PVP, M_w: 1 300 000, Aladdin Industrial Corporation) and poly(3,4-ethylenedioxythiophene):poly(styrene sulfonate) (PEDOT:PSS) dispersion liquid (1.05 wt% dispersion in water, Shanghai OE chemicals Ltd., China) were used in this work. *N*,*N*-dimethylformamide (DMF), tetrahydrofuran (THF), and ethanol were obtained from Sinopharm Chemical Reagent. Acetone was obtained from Laiyang Fine Chemical Factory, China. Other materials used include 1-ethyl-3-methylimidazole acetate (Sun Chemical Technology. Co., Ltd), carbon nanotube slurry (CNTS, 10 wt% dispersion in water, Qingdao Haoxin New Energy Technology Co., Ltd., China), ethylene glycol (EG, Sinopharm Chemical Reagent Co., Ltd) and copper foil tape (double-sided conductive, Dongguan Xinshi Packaging Materials Co. Ltd., China).

2.2 Preparation of solutions for electrospinning and cast films

PVDF solution (22 wt%) was prepared by dissolving PVDF powder in an acetone–DMF solvent mixture (1/1 w/w) and then stirring the mixture with a magnetic stir bar for 4 h at 50 °C. For preparation of the TPU solution (12 wt%), the polymer was dissolved in DMF-THF (1/1 w/w) at room temperature and was continuously stirred for at least 3 h. The precursor solution for the conductive nanofiber membrane (CNFM) was prepared by dissolving PVP (13 wt%) in PEDOT:PSS dispersion liquid (50 wt%), ethyl alcohol (30 wt%), and EG (5 wt%). Subsequently, ionic liquid (1-ethyl-3-methylimidazole acetate, 2 wt%) was added to the solution. After stirring for 3 h, the solution became homogeneous.

2.3 Fabrication of the NG and cast film

A schematic of the electrospinning process is displayed in Fig. S1.† The spinning solution was loaded into a syringe, and the flow rate of the solution was regulated at 1 mL h^{-1} by using a syringe pump (LSP01-1A, Baoding Longer Precision Pump Co. Ltd., China). A drum collector (10 cm in diameter, 20 cm in length, 90 rpm rotating speed) was placed 15 cm (collect distance) away from the needle to collect the nanofibers, and a 15 kV voltage was applied between the needle and the drum collector. The syringe pump was fixed on a slide rail which was driven by a linear motor and provided reciprocating motion at a speed of 10 cm s^{-1}. Thus, a two-dimensional uniform electrospun nanofiber membrane was obtained.

Fig. S2† displays the fabrication steps of the designed NG device. First, the TPU NFM was fabricated as a substrate (Fig. S2a†), and an effective area for the NG was selected and delineated with a pen. Then, copper foil tape was pasted as the bottom outer electrode, and carbon nanotube slurry (CNTS) was coated uniformly in the delineated area as the bottom electrode (Fig. S2b†). When the CNTS was in a semi-dry state, a PVDF NFM with a thickness of about 150 μm was fabricated as the working layer (Fig. S2c†). After that, a layer of PEDOT:PSS-PVP CNFM was covered on the PVDF NFM as the top electrode (Fig. S2d†). Then, copper foil tape was pasted as the top output electrode (Fig. S2e†). Finally, the NG device was cut from the area marked by a dotted line (Fig. S2f†). For comparison, a piece of cast film of PVDF was obtained from the spreading PVDF solution (22 wt%) on glass at room temperature.

2.4 Characterization

The morphologies and microstructures of the NFMs were characterized using a scanning electron microscope (SEM, JEOL, JSM-7500F). The fiber diameter was calculated using Nano Measurer 1.2.5 software. For crystal structure analysis, X-ray diffraction (XRD) patterns were obtained on a diffractometer (Rigaku, SmartLab). The output currents of the NG were measured by a picoammeter (Keithley 6487). The output voltage of the NG was measured by an oscilloscope (Agilent DSO-X 3024 A), and the charging voltages of the capacitor were recorded by a digital multimeter (Rigol DM 3058). To generate piezoelectric power from the NG, we used a home-made pressure apparatus which could exert periodic impact force; the schematic and working principle of this apparatus are shown in Fig. S3a in the ESI.† In order to measure the output electric signal of the NG upon bending deformation, we used a home-made linear motor for bending and unbending with a maximum displacement of 4 cm. To generate pyroelectric power from the PVDF NFM, a flexible commercial polyimide heater was used to rapidly change the temperature of the NG. The temperature of the PVDF NFM was measured by a K-type thermocouple. The coupling of the piezoelectric and pyroelectric outputs was determined by using the self-made pressure apparatus and the heater at the same time. The tensile behavior of the NG was measured by an Instron 3300 Universal Testing Systems instrument at a stretching speed of 1 mm min^{-1}.

3. Results and discussion

3.1 The basic characterization of the NG

Fig. 1a shows a schematic of the flexible energy conversion NG and its photograph (inset). The NG was mainly composed of four layers, as shown in the cross-section view of the device in Fig. 1b; three of these were electrospun fiber layers consisting of randomly oriented fibers. The electrospun TPU NFM (Fig. 1c) acted as a substrate and the load layer of the CNTs; its thickness was about 120 to 140 μm. The TPU fibers had an average diameter of 0.79 μm. The bottom electrode was a CNTs layer which was obtained from a dry carbon nanotube slurry (CNTS)

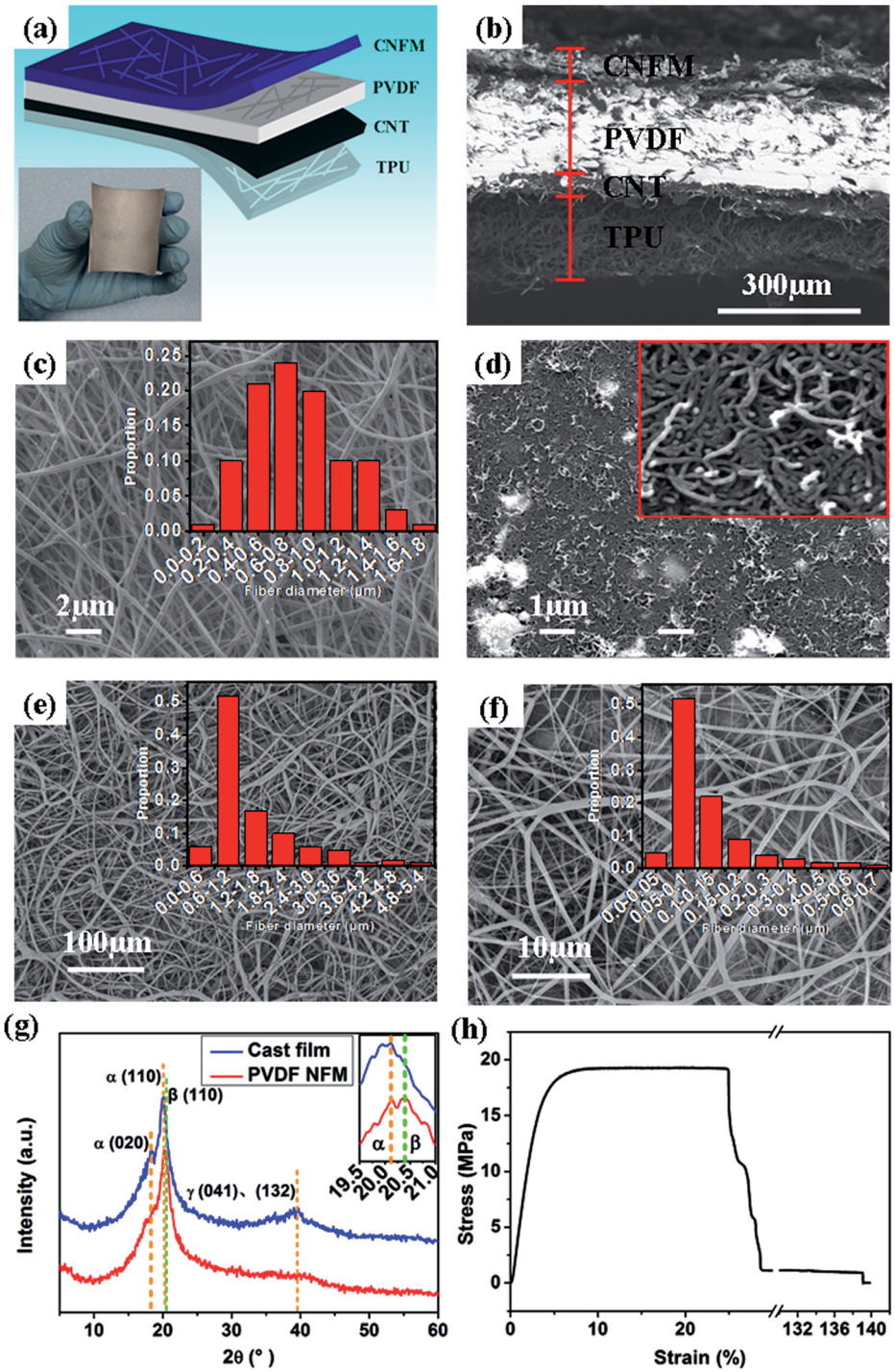

Fig. 1 (a) Schematic of the self-powered non-woven NG composed of the TPU NFM substrate, CNT bottom electrode, PVDF NFM, and CNFM top electrode. A photograph of the NG is shown in the inset. (b) Cross-section SEM image of the NG. SEM images and bar charts (insets) of the fiber size distributions of the (c) TPU NFM, (e) PVDF NFM, and (f) CNFM. (d) SEM image of the CNT layer which was coated on the TPU NFM. (g) XRD patterns of the electrospun PVDF NFM and PVDF cast film. (h) The stress–strain curve of the entire NG.

coating. As shown in Fig. 1d, the CNTs were uniformly and densely attached to the TPU NFM, and the surface conductivity of the CNTs layer was about 4.417×10^{-3} S cm^{-1}. Furthermore, the carbon nanotube slurry pasted the PVDF NFM and TPU NFM together well. An electrospun PEDOT:PSS-PVP CNFM doped with ionic liquid introduced in our previous work[34] with a surface conductivity of about 1.27×10^{-4} S cm^{-1} was introduced as a flexible top electrode. The thickness of the PEDOT:PSS-PVP CNFM was about 40 μm, and its average fiber diameter was about 130 nm (see Fig. 1f). In contrast with previously reported studies[35–39] in which nanofibers were covered with aluminum foil as an electrode, the PEDOT:PSS-PVP CNFM did not damage the PVDF nanofibers and adhered to the PVDF NFM very well because both layers are composed of electrospun non-woven nanofibers. More importantly, both electrodes used in this work showed outstanding flexibility; thus, they are suitable for use in wearable electronic textiles.

As the core part of the NG, the PVDF NFM acted as the piezoelectric and pyroelectric material, with a thickness of about 150 μm. As can be seen from Fig. 1e, the electrospun PVDF nanofibres had an average diameter of 1.42 μm and a diameter distribution (standard deviation) of 0.98 μm. The crystal phase of the PVDF NFM was examined using XRD. For comparison, the XRD pattern of the PVDF cast film is also shown in Fig. 1g. As can be seen from the curves, the PVDF cast film exhibited prominent peaks at $2\theta = 18.8°$ and 20.2°, corresponding to the (020) and (110) reflections of the α phase, respectively,[35] and a peak at $2\theta = 39.4°$, corresponding to the (041) and (132) reflections of the γ phase.[38] In the case of the electrospun PVDF NFM, these peaks were sharply decreased; meanwhile, a new peak appeared at $2\theta = 20.4°$ corresponding to the (110) reflections of the β phase formation,[36,39] indicating that electrospinning favours the formation of β phase crystalline PVDF, which is in agreement with other reports.[29,30] This is due to simultaneous poling, elongation forces, stretching, and rapid evaporation of the solvent during the electrospinning process, which promotes the formation of the β phase.[35,37] In addition, the β phase molecular chain has preferred orientation along the fiber axis and the electro-active dipoles are perpendicular to the chain; as a result, the electro-active dipoles of PVDF orientate along the thickness direction of the PVDF NFM under the induction of the applied electrospinning electric field,[31,33] as shown in Fig. 2a.

Fig. 1h shows the stress–strain curve obtained from tensile testing of the non-woven NG. The overall tensile strength of the NG is about 19.27 MPa. The NG is composed of multiple layers; the PVDF NFM layer broke first, with an elongation of 24.93%. Subsequently, the CNFM layer broke, and finally, the TPU layer broke with an elongation of 139.25%. This demonstrates the damage-resistant properties of the device when acting as a wearable NG.

3.2 The piezoelectric outputs of the NG in mechanical impact and bend situations

Upon repetitively impacting and releasing the NG (the effective size of the NG was 4 cm × 4 cm) by a home-made pressing

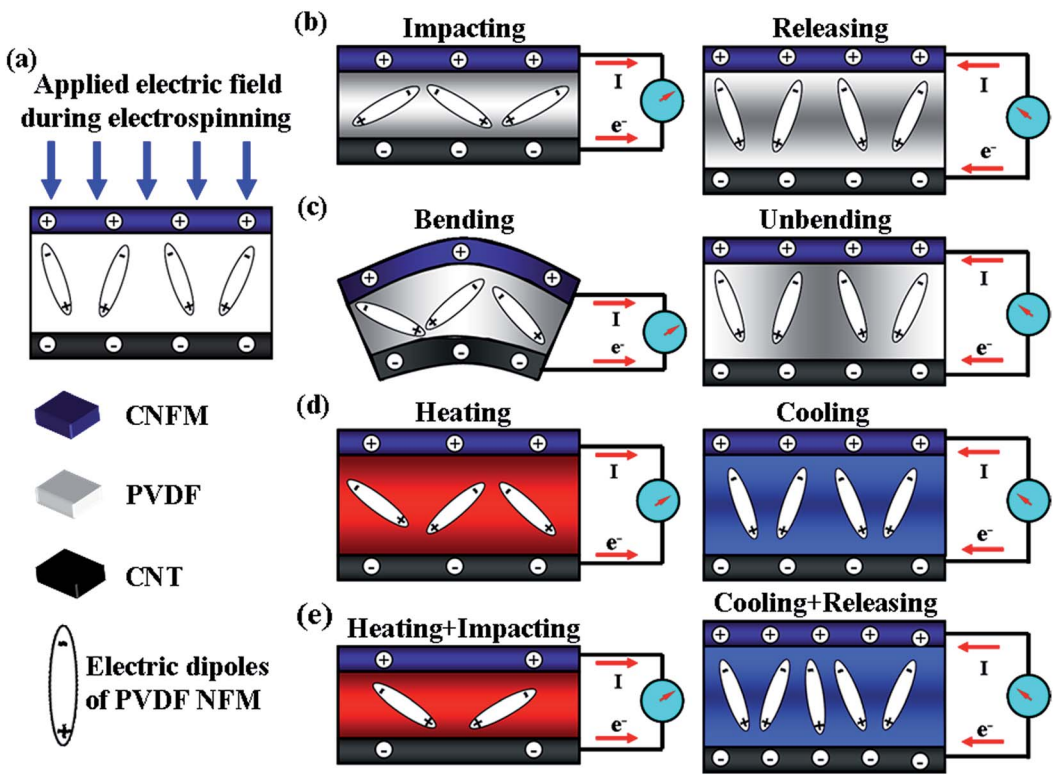

Fig. 2 (a) Schematic of the orientation of the electric dipoles which formed in the electrospinning process of PVDF. Principles of (b) piezoelectric output in the impacting/releasing mode, (c) piezoelectric output in the bending/unbending mode, (d) pyroelectric output in the heating/cooling mode, and (e) hybrid piezoelectric–pyroelectric output in the impacting during heating and releasing during cooling modes.

apparatus with a frequency of 1.2 Hz (see Fig. S3a and Video S1 in the ESI†), the output current was detected and is shown in Fig. 3a; it exhibits typical piezoelectric signals. When the NG was subjected to compression, a pulse current/voltage signal (referred to as the first signal) was detected; then, when the impact was released, an opposite pulse signal (referred to as the second signal) was recorded. In order to elucidate the experimental results, we show the energy harvesting mechanism of the NG in Fig. 2. In the absence of perturbation, no output current or voltage is observed. Because the electric dipoles randomly oscillate within a degree from their respective aligning axes, the total average strength of the spontaneous polarization from the electric dipoles is constant in this case.[28,40] When mechanical impact is applied on the NG, the PVDF NFM is compressed; the total spontaneous polarization decreases significantly, and a flow of electrons (the first signal) from the bottom electrode to the top electrode is generated due to the decrease in the induced charges. Conversely, when the impact is released, an opposite signal (the second signal) is observed because the polarization is recovered (Fig. 2b). Under the condition of zero load impedance, the piezoelectric current I_{pizeo} can be expressed by the equation

$$I_{\text{piezo}} = d_{33} A \mathrm{d}\sigma/\mathrm{d}t \quad (1)$$

where d_{33}, A and $\mathrm{d}\sigma/\mathrm{d}t$ are the piezoelectric coefficient, effective area of the device and rate of mechanical stress change, respectively.[41]

The effects of impact frequency on the electrical output were also investigated. As can be seen from Fig. 3b, under an impact of 0.65 Hz, the average positive/negative peak current output was about 0.54 μA/−0.21 μA. When the frequency was 1.2 Hz, the positive/negative output became 2.32 μA/−0.78 μA. After reaching the maximum at a frequency of 3 Hz, the output current reached 3.76 μA/−0.94 μA. Similarly, the output voltage during impact increased with the frequency, as shown in Fig. S4.† According to the equation.

$$W_{\text{e}} = \int VI\mathrm{d}t \quad (2)$$

where V and I are the measured output voltage and current, respectively,[29] the electrical energies (W_{e}) generated from one impact-release cycle on the NG at 0.65, 1.2, and 3 Hz were calculated as 0.78, 2.39 and 2.85 μJ, respectively. For the impact frequencies of 1.2 and 3 Hz, the NG could directly light a white LED, as shown in Video S2.† The variation of the electrical outputs caused by the impact frequency originates from the initial impact speed, which leads to different values of $\mathrm{d}\sigma/\mathrm{d}t$ for the NG.[29] For the impact frequencies of 0.65, 1.2, and 3 Hz, the initial impact speeds were about 48.5, 65.9, and 72.5 mm s^{-1}, respectively. A faster speed results in a higher impact energy and impact force, which leads to larger values of $\mathrm{d}\sigma/\mathrm{d}t$ for the NG. For comparison, a cast PVDF film-based NG was also measured under the same impact at a frequency of 1.2 Hz; the average peak current output was about 15.23 nA (see Fig. 3c). There is an obvious decrease of about two orders of magnitude in the current output compared with that of the electrospun PVDF NG. The weak piezoelectric output is probably due to the low β-phase content in the cast film and the dense structure of the cast film, which is less deformed by the impact compared with the electrospun nanofiber membranes.[29]

Piezoelectric current output also can be generated from mechanical bending of the NG. As shown in Fig. 3d and Video S3,† the mechanical bending was caused by a home-made liner motor. The output currents of the NG (effective size was 4 cm × 6 cm) were generated at a minimum horizontal distance length

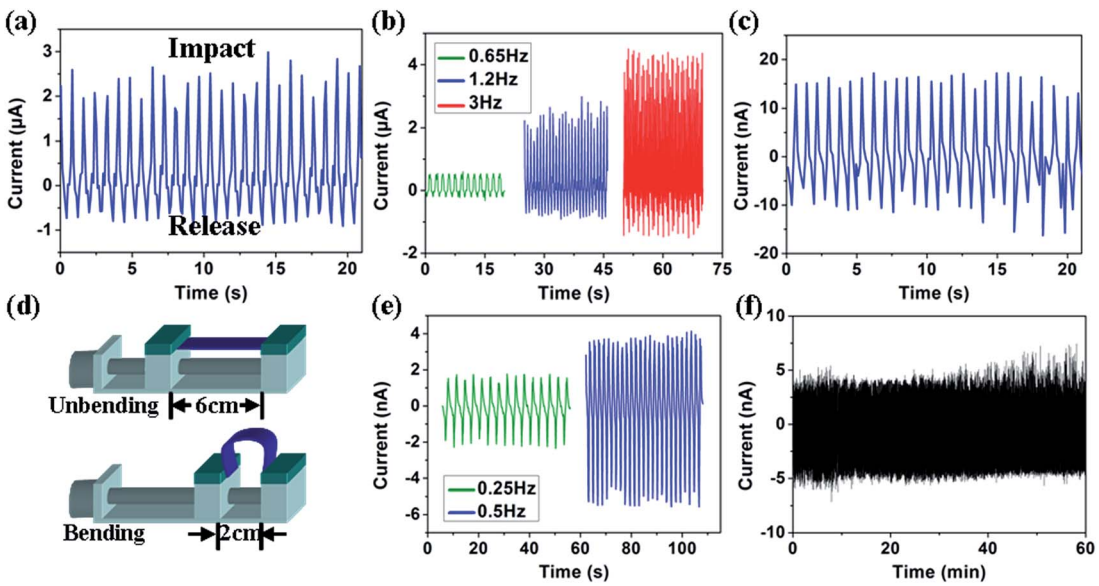

Fig. 3 (a) Output current of the non-woven NG under 1.2 Hz repeated compressive impacts. (b) Output current of the NG subject to different impact frequencies. (c) Output current of the cast PVDF film-based NG under 1.2 Hz repeated compressive impacts. (d) Schematics of the mechanical bending and unbending of the NG caused by a self-made liner motor. (e) The measured output currents of the mechanical bending at frequencies of about 0.25 Hz and 0.5 Hz. (f) The durability test results of the NG subjected to a bending frequency of 0.5 Hz.

of 2 cm from an originally 6 cm long device at bending frequencies of about 0.25 and 0.5 Hz. As suggested in Fig. 3e, a pulse current accompanied by an opposite pulse current signal was detected when the NG was operated on a bending and release strain mode. Fig. 2c shows the energy harvesting mechanism of the mechanical bending. Bending leads to strain of the NFM and a decrease of electric polarization along the poling direction.[14] To balance the induced charges, a flow of electrons (the positive current) from the bottom electrode to the top is generated. As the external strain is relieved by the unbending motion, the electric polarization decreases and the electrons flow in reverse.[37] The average positive and negative peak short currents were 1.61 and −2.16 nA, respectively, when the NG was bent at a frequency of 0.25 Hz. As the bending frequency increased to 0.5 Hz, the positive and negative current increased to 3.63 and −5.20 nA, respectively. The increase of the bending frequency results in a greater deformation rate and a larger value of $d\sigma/dt$ in eqn (1), which leads to the increase of the output current.

As can be seen from Fig. 3b and e, the current output during impact was much higher for the NG during bending. This is because the process of bending deformation of the NG lasted 2 s (0.25 Hz) and 1 s (0.5 Hz); however, the impacting deformation process was completed in an instant. In addition, the spontaneous polarization is parallel to the thickness direction of the electrospun PVDF; as a result, the deformation of the NG in the thickness direction caused by the bending is much smaller than that caused by impacting. Therefore, during impact, the $d\sigma/dt$ value in the thickness direction of the electrospun PVDF membrane is much larger than that under bending; thus, the current output in the impact mode is much higher than in the bending mode. Also, the output current shows different sensitivities to input frequency during bending and impact. The reason is that the bending frequency directly affects the stress changing rate, resulting in a change in the output current; meanwhile, the impact frequency influences the impact speed and thus indirectly affects the stress changing rate, leading to the change in output current.

To confirm the mechanical durability of the non-woven NG, the NG was bent and unbent for 1 hour (about 1800 cycles) at a frequency of 0.5 Hz. The result is shown in Fig. 3f; the comparably stable output current indicates the mechanical durability of the PVDF NFM NG fabricated by electrospinning. The piezoelectric energy generated by the NG was able to charge a capacitor and then power an LED, as shown in Fig. S5.†

3.3 The pyroelectric output and hybrid piezoelectric–pyroelectric electrical outputs of the NG

In order to test the current output of the PVDF NFM-based NG for converting thermal energy, the NG (effective size 4 cm × 4 cm) was attached on the surface of a flexible polyimide heater, as shown in Fig. S3b in ESI.† Fig. 4a and b show the changes in temperature of the NG and the corresponding differential curves. When the NG was heated from 313 to 319 K, positive current pulses (20 nA) could be observed, as shown in Fig. 4c. The opposite current (−16 nA) was observed when the temperature returned to 313 K. Also, the corresponding output peak voltage was about 0.01 V/−0.087 V, as shown in Fig. S6.† In order to elucidate the experimental results, the mechanism of the pyroelectric generator is displayed in Fig. 2d. When a change in temperature from a lower temperature to a higher temperature is applied to the NG, the electric dipoles will oscillate within a larger degree of spread angles due to higher thermal motion, which results in a decrease of spontaneous polarization.[39] Thus, a flow of electrons from the bottom electrode to the top electrode is generated because the quantity of induced charges in the electrodes is reduced. Consequently, thermal cooling enhances spontaneous polarization because the electric dipoles oscillate within a smaller angle, resulting in a flow of electrons in the opposite direction. Usually, the pyroelectric current I_{pyro} can be determined by the equation

$$I_{pyro} = pA\,dT/dt \quad (3)$$

where p, A and dT/dt are the pyroelectric coefficient, effective area, and the rate of temperature change, respectively.[42] Eqn (3) indicates that the output current linearly increases with increasing rate of temperature change, which is consistent with the experimental results shown in Fig. 4b and c. Also, the pyroelectric output current of the cast PVDF film was measured under the same test conditions; as shown in Fig. S7,† the current output was drastically reduced relative to that of the electrospun PVDF NG. Fig. 4d shows the pyroelectric output currents obtained upon heating the NG for 3 seconds and then cooling for 5 s when the flexible polyimide heater and the NG were at different initial temperatures. It can be clearly seen that the output peak currents significantly increased with increasing initial temperature. This indicates that the pyroelectric coefficient increases with increasing temperature; this result is similar to other studies.[14] Moreover, we tested the output pyroelectric currents of the NG in different shapes or under different mechanical stresses by holding the NG on static curved surfaces with different bending radii (as the illustration shows); the results (Fig. 4e) show that there were no significant changes in the NG response. This indicates that the pyroelectric electrical output will not be affected when the flexible NG is attached to heat sources with various shapes.

Moreover, we tested the hybrid piezoelectric–pyroelectric electrical output of the electrospun PVDF NFM for the first time in this work. In order to implement this test, the NG was heated by the flexible polyimide heater and impacted by the self-made pressing apparatus simultaneously (a schematic is exhibited in Fig. S3c in the ESI†). As shown in Fig. 4f, the total output signal is a coupling of piezoelectric and pyroelectric effects. Also, the maximum peak is enhanced by both effects. The coupling current can be expressed as[28]

$$I_{piezo+pyro} = d_{33}A\,d\sigma/dt + pA\,dT/dt \quad (4)$$

which is the sum of I_{piezo} (eqn (1)) and I_{pyro} (eqn (3)). When the NG is impacted during heating, the spontaneous polarization is smaller than that when it is heated or impacted individually.

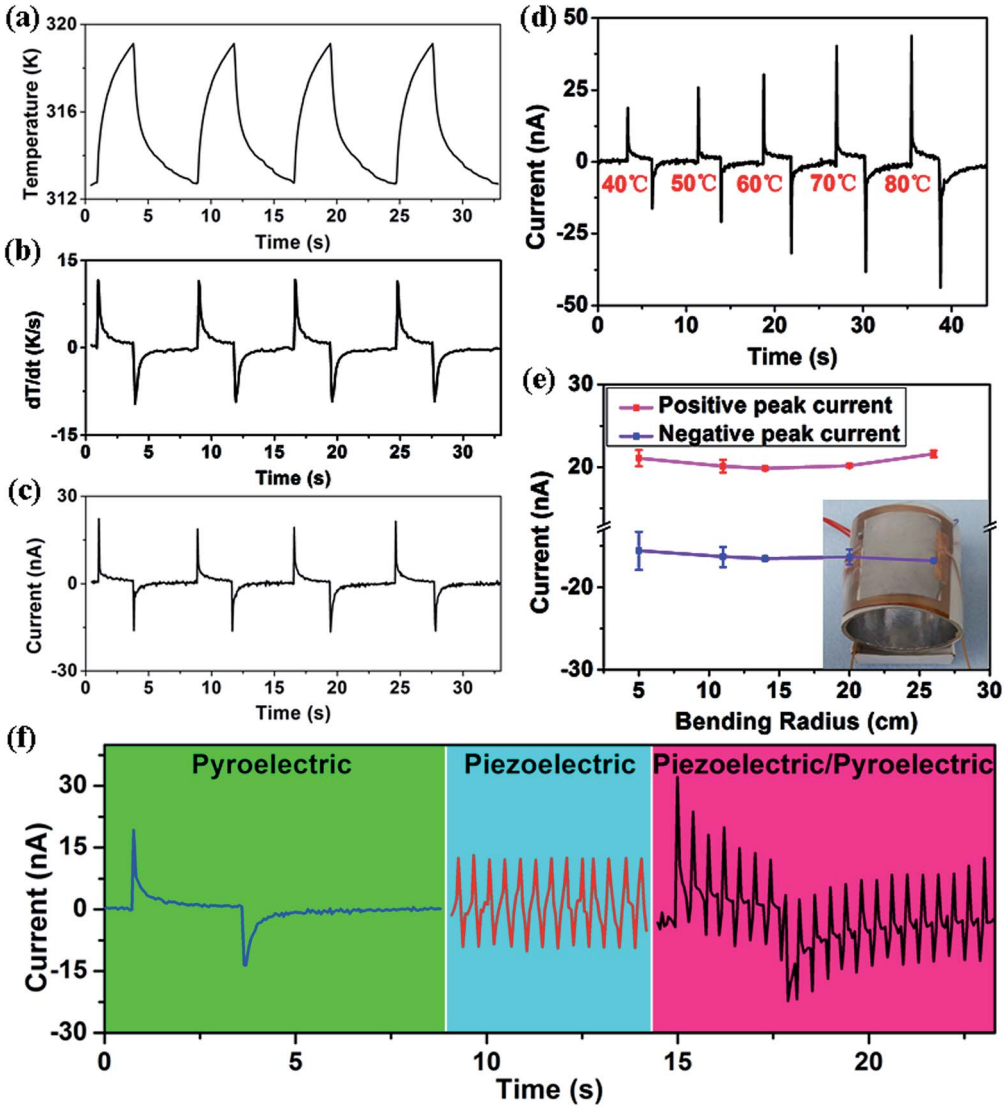

Fig. 4 (a) Changes in temperature of the NFM-based NG, (b) the corresponding differential curve, and (c) the corresponding output current. (d) Measured output currents of the NG when heated from different initial temperatures. (e) The output peak current of the NG in different shapes or under different mechanical stresses by holding the NG on static curved surfaces with different bending radii. (f) The pyroelectric output current when heating the NG for 3 seconds and cooling for 5 seconds. The piezoelectric output current when impacting the NG at a frequency of 2.5 Hz. The hybrid piezoelectric–pyroelectric output current when heating/cooling and impacting the NG simultaneously.

In contrast, the spontaneous polarization is enhanced upon impact release during cooling of the NG (as shown in Fig. 2e). This indicates that reasonable control of mechanical and thermal effects can increase the output of electrical energy.

3.4 Applications for harvesting energy from human motions and cold/hot airflows

This flexible and lightweight self-powered non-woven NG is particularly suitable for use as a wearable power source for personal electronic equipment to provide sustainable power. Human motions, such as walking, jumping, and arm swinging, can result in mechanical strain of the NG, which can generate piezoelectric current output. In Fig. 5a, we show a photograph and output current of the NG being struck by hand. When the NG was subjected to hand striking, the maximum positive and negative peak currents were about 0.32 and −0.15 μA, respectively. Obviously, the electrical output is uneven due to the instability of manual operation. As shown in Fig. 5b, the NG was integrated into the insole of a shoe. The maximum positive and negative peak current output which were generated from the non-woven NG during walking were about 26.83 and −23.43 nA, respectively. When this shoe was worn while running, the output currents significantly increased, reaching 78.55 nA (maximum positive peak current output) and −47.36 nA (maximum negative peak current output), respectively. To obtain piezoelectric currents from bending motions of the body, the NG was fixed to an elbow with tape; as shown in Fig. 5c, the output currents were measured at different arm swinging frequencies. At the frequency of about 0.4 to 0.6 Hz (low

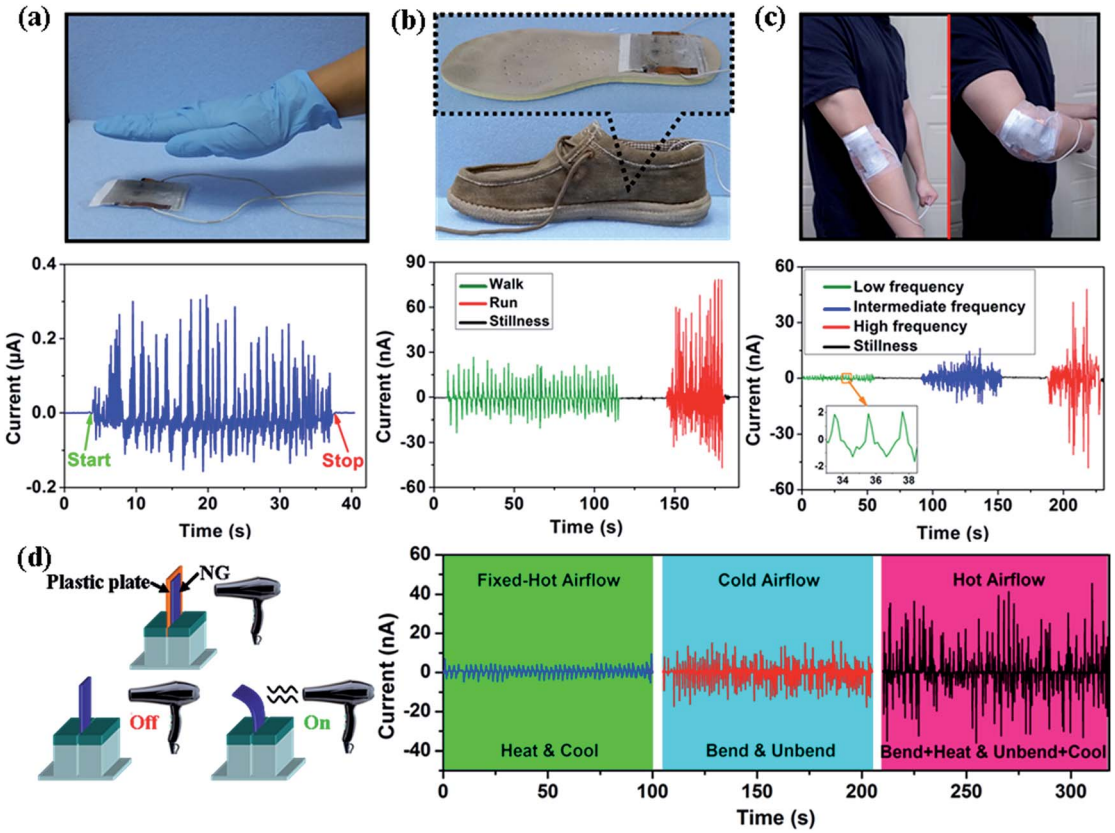

Fig. 5 (a) Photograph of the NG being struck by hand and the corresponding output current. (b) Photograph of the NG integrated into an insole and the output currents generated by walking and running. (c) Photograph of the device fixed to an elbow and the output currents generated by arm swinging at low frequency, intermediate frequency, and high frequency. (d) Schematic of the scavenging of mechanical and thermal energies of cold/hot airflows. Output currents for a hot airflow periodically turned on and off when the NG was fixed on a plastic plate, when a cold airflow was periodically turned on and off with bending, and when a hot airflow was periodically turned on and off with bending.

frequency), corresponding to the frequency of arm swing in the case of walking, the output current ranged from −1.7 nA to 2 nA. When the frequency of arm swing was increased to 1.1 to 1.3 Hz (intermediate frequency, equivalent to jogging), the range of current output became −13.78 to 16.24 nA. Further increasing the frequency to 1.8 to 2.9 Hz (high frequency, equivalent to fast running) led to the output current reaching −47.7 nA to 48.4 nA. Currently, many studies have shown that electrospun NFMs are suitable for textile fabrics,[43–45] and large area NFMs can be prepared using existing electrospinning technology;[46] thus, it is possible to fabricate self-powered clothes, carpets, *etc.* using electrospun non-woven fibers.

Many exhaust gases contain both mechanical and thermal energies; in this work, we further demonstrate the capability of the flexible NG to harvest mechanical and thermal energies from cold and hot airflows individually and simultaneously. To enable free vibration of the NG by airflow, one end of the NG was fixed to a metal fixture. To mimic cold and hot air flows, we passed cold (room temperature: 24 °C) and hot (120 °C) flows over the NG using a household hair dryer, as shown in the schematic in Fig. 5d. In the data graph, we show the pyroelectric current output (the blue line) caused by the periodic hot airflow heating and natural air cooling (the NG was fixed on a plastic plate, see the top of the schematic); the piezoelectric current output (the red line) caused by periodically turning the cold airflow on (bending) and off (unbending); and the hybrid piezoelectric–pyroelectric current output (the black line) caused by periodically turning the hot airflow on (bending and heating) and off (unbending and cooling). As can be seen from the results, the hybrid output current was enhanced under the combined action of piezoelectric and pyroelectric effects. This periodic hot air flow situation is similar to the exhaust emissions of a car, which has been proved to be an effective method to drive a hybrid NG to generate electricity.[14]

4. Conclusion

In summary, a self-powered non-woven NG based on a flexible hybrid piezoelectric–pyroelectric nanogenerator which consisted of an electrospun PVDF NFM, a TPU NFM substrate, PEDOT:PSS-PVP CNFM and CNT coating electrodes was developed. The electrical outputs of the NG under different frequencies of applied mechanical impact and bending were measured; it was found that at impact frequencies of 1.2 and 3 Hz, the NG could directly light a white LED. Also, current output of the NG induced by a thermal gradient was successfully detected, and its stable pyroelectric current outputs in different shapes or under different mechanical stresses were

demonstrated. Furthermore, a hybrid piezoelectric and pyroelectric current was obtained by impacting (releasing) and heating (cooling) the NG simultaneously; the electrical energy generated by the NG could be used to charge a capacitor and drive a white LED. Based on the flexible structure of the nonwoven NG, its applications for harvesting energy from human motions and cold/hot airflows were suggested, and we demonstrated that this flexible hybrid piezoelectric–pyroelectric NG has potential applications in self-powered electronic textiles.

Conflicts of interest

There are no conflicts to declare.

Acknowledgements

This work was supported by the National Natural Science Foundation of China (51673103, 51373082 and 51703102), the Taishan Scholars Program of Shandong Province, China (ts20120528), the Shandong Provincial Key Research and Development Plan (2016GGX102011), and the Shandong Provincial Natural Science Foundation, China (ZR2016EMB09).

References

1 N. Wu, H. Jiang, W. Li, S. Lin, J. Zhong, F. Yuan, L. Huang, B. Hu and J. Zhou, *J. Mater. Chem. A*, 2017, **5**, 12787–12792.
2 X. Chen, Y. Song, H. Chen, J. Zhang and H. Zhang, *J. Mater. Chem. A*, 2017, **5**, 12361–12368.
3 J. Wang, C. Wu, Y. Dai, Z. Zhao, A. Wang, T. Zhang and Z. L. Wang, *Nat. Commun.*, 2017, **8**, 88.
4 Z. L. Wang, J. Chen and L. Lin, *Energy Environ. Sci.*, 2015, **8**, 2250–2282.
5 J. Chen and Z. L. Wang, *Joule*, 2017, **1**, 480–521.
6 J. Chen, Y. Huang, N. Zhang, H. Zou, R. Liu, C. Tao, X. Fan and Z. L. Wang, *Nat. Energy*, 2016, **1**, 16138.
7 N. Zhang, J. Chen, Y. Huang, W. Guo, J. Yang, J. Du, X. Fan and C. Tao, *Adv. Mater.*, 2016, **28**, 263–269.
8 J. Chen, G. Zhu, W. Yang, Q. Jing, P. Bai, Y. Yang, T. C. Hou and Z. L. Wang, *Adv. Mater.*, 2013, **25**, 6094–6099.
9 Z. L. Wang, *Mater. Today*, 2017, **20**, 74–82.
10 Z. Lin, J. Chen, X. Li, Z. Zhou, K. Meng, W. Wei, J. Yang and Z. L. Wang, *ACS Nano*, 2017, **11**, 8830–8837.
11 L. Jin, J. Chen, B. Zhang, W. Deng, L. Zhang, H. Zhang, X. Huang, M. Zhu, W. Yang and Z. L. Wang, *ACS Nano*, 2016, **10**, 7874–7881.
12 B. Zhang, J. Chen, L. Jin, W. Deng, L. Zhang, H. Zhang, M. Zhu, W. Yang and Z. L. Wang, *ACS Nano*, 2016, **10**, 6241–6247.
13 N. Zhang, C. Tao, X. Fan and J. Chen, *J. Mater. Res.*, 2017, **32**, 1628–1646.
14 Y. J. Ko, D. Y. Kim, S. S. Won, C. W. Ahn, I. W. Kim, A. I. Kingon, S. H. Kim, J. H. Ko and J. H. Jung, *ACS Appl. Mater. Interfaces*, 2016, **8**, 6504–6511.
15 H. Guo, X. He, J. Zhong, Q. Zhong, Q. Leng, C. Hu, J. Chen, L. Tian, Y. Xi and J. Zhou, *J. Mater. Chem. A*, 2014, **2**, 2079–2087.
16 L. Zhang, B. Zhang, J. Chen, L. Jin, W. Deng, J. Tang, H. Zhang, H. Pan, M. Zhu, W. Yang and Z. L. Wang, *Adv. Mater.*, 2016, **28**, 1650–1656.
17 L. Zheng, G. Cheng, J. Chen, L. Lin, J. Wang, Y. Liu, H. Li and Z. L. Wang, *Adv. Energy Mater.*, 2015, **5**, 1501152.
18 Y. Yang, G. Zhu, H. Zhang, J. Chen, X. Zhong, Z. H. Lin, Y. Su, P. Bai, X. Wen and Z. L. Wang, *ACS Nano*, 2013, **7**, 9461–9468.
19 J. Park, Y. Lee, M. Ha, S. Cho and H. Ko, *J. Mater. Chem. B*, 2016, **4**, 2999–3018.
20 W. Seung, M. K. Gupta, K. Y. Lee, K. S. Shin, J. H. Lee, T. Y. Kim, S. Kim, J. Lin, J. H. Kim and S. W. Kim, *ACS Nano*, 2015, **9**, 3501–3509.
21 K. N. Kim, J. Chun, J. W. Kim, K. Y. Lee, J. U. Park, S. W. Kim, Z. L. Wang and J. M. Baik, *ACS Nano*, 2015, **9**, 6394–6400.
22 Z. Li, J. Shen, I. Abdalla, J. Yu and B. Ding, *Nano Energy*, 2017, **36**, 341–348.
23 W. Wu, S. Bai, M. Yuan, Y. Qin, Z. L. Wang and T. Jing, *ACS Nano*, 2012, **6**, 6231–6235.
24 P. Bai, G. Zhu, Q. Jing, J. Yang, J. Chen, Y. Su, J. Ma, G. Zhang and Z. L. Wang, *Adv. Funct. Mater.*, 2014, **24**, 5807–5813.
25 J. Yang, J. Chen, Y. Su, Q. Jing, Z. Li, F. Yi, X. Wen, Z. Wang and Z. L. Wang, *Adv. Mater.*, 2015, **27**, 1316–1326.
26 W. Yang, J. Chen, X. Wen, Q. Jing, J. Yang, Y. Su, G. Zhu, W. Wu and Z. L. Wang, *ACS Appl. Mater. Interfaces*, 2014, **6**, 7479–7484.
27 F. Yi, L. Lin, S. Niu, P. K. Yang, Z. Wang, J. Chen, Y. Zhou, Y. Zi, J. Wang, Q. Liao, Y. Zhang and Z. L. Wang, *Adv. Funct. Mater.*, 2015, **25**, 3688–3696.
28 J. H. Lee, K. Y. Lee, M. K. Gupta, T. Y. Kim, D. Y. Lee, J. Oh, C. Ryu, W. J. Yoo, C. Y. Kang, S. J. Yoon, J. B. Yoo and S. W. Kim, *Adv. Mater.*, 2014, **26**, 765–769.
29 J. Fang, X. Wang and T. Lin, *J. Mater. Chem.*, 2011, **21**, 11088–11091.
30 A. Gheibi, M. Latifi, A. A. Merati and R. Bagherzadeh, *J. Polym. Res.*, 2014, **21**, 469.
31 W. A. Yee, M. Kotaki, Y. Liu and X. Lu, *Polymer*, 2007, **48**, 512–521.
32 J. Zheng, A. He, J. Li and C. C. Han, *Macromol. Rapid Commun.*, 2007, **28**, 2159–2162.
33 D. Mandal, S. Yoon and K. J. Kim, *Macromol. Rapid Commun.*, 2011, **32**, 831–837.
34 D. P. Lin, H. W. He, Y. Y. Huang, W. P. Han, G. F. Yu, X. Yan, Y. Z. Long and L. H. Xia, *J. Mater. Chem. C*, 2014, **2**, 8962–8966.
35 D. Dhakras, V. Borkar, S. Ogale and J. Jog, *Nanoscale*, 2012, **4**, 752–756.
36 J. Fang, H. Niu, H. Wang, X. Wang and T. Lin, *Energy Environ. Sci.*, 2013, **6**, 2196–2202.
37 H. Yu, T. Huang, M. Lu, M. Mao, Q. Zhang and H. Wang, *Nanotechnology*, 2013, **24**, 405401.
38 Y. J. Park, Y. S. Kang and C. Park, *Eur. Polym. J.*, 2005, **41**, 1002–1012.
39 S. Wang, Z. L. Wang and Y. Yang, *Adv. Mater.*, 2016, **28**, 2881–2887.
40 Y. Yang, J. H. Jung, B. K. Yun, F. Zhang, K. C. Pradel, W. Guo and Z. L. Wang, *Adv. Mater.*, 2012, **24**, 5357–5362.

41 C. Wan and C. R. Bowen, *J. Mater. Chem. A*, 2017, **5**, 3091–3128.
42 Y. Yang, H. Zhang, G. Zhu, S. Lee, Z. H. Lin and Z. L. Wang, *ACS Nano*, 2013, **7**, 785–790.
43 S. Lee and S. K. Obendorf, *Text. Res. J.*, 2007, **77**, 696–702.
44 M. Ma, Y. Mao, M. Gupta, K. K. Gleason and G. C. Rutledge, *Macromolecules*, 2005, **38**, 9742–9748.
45 R. Bagherzadeh, M. Latifi, S. S. Najar, M. A. Tehran, M. Gorji and L. Kong, *Text. Res. J.*, 2012, **82**, 70–76.
46 M. Yu, R. H. Dong, X. Yan, G. F. Yu, M. H. You, X. Ning and Y. Z. Long, *Macromol. Mater. Eng.*, 2017, **302**, 1700002.